

Low-Profile and Low-Volume Split-Distributed Resonators and Filters

SENAD BULJA¹, (Senior Member, IEEE), AND DMITRY KOZLOV², (Member, IEEE)

¹Nokia Bell Labs, Dublin 15, D15 Y6NT Ireland

²Nokia Technology Center, 89081 Ulm, Germany

Corresponding author: Senad Bulja (senad.bulja@gmail.com)

ABSTRACT A new class of low-profile resonators, named split-distributed resonators is introduced in this paper. The newly proposed resonator family features high quality Q-factors and relies not only on the coupling among the constituent resonant elements, but the constituent elements themselves are also made in the distributed form. This, in comparison with the standard distributed resonator, caters for extremely low profiles, while allowing for a more uniform distribution of the electromagnetic fields inside the resonant cavity and hence higher unloaded quality factors. Furthermore, a uniform distribution of the electromagnetic fields facilitates a tremendous reduction of the resonator volume. As an experimental verification, two 5-pole band-pass filters using different realizations of individual resonant elements are designed and fabricated. The filters operate at a centre frequency of 1.8 GHz with a percentage bandwidth of 2%. The individual split-distributed resonator of these filters consists of 9 resonant elements, where each element is a distributed resonator of the second order and fourth order respectively. The measured insertion losses of the filters are in a good agreement with the values predicted by the simulations.

INDEX TERMS Filters, quality factor, resonator.

I. INTRODUCTION

Filters are of vital importance to all telecommunication systems. Even though the fundamental principles of the operation of filters have been known since the second part of the 20th century, novel filter realisations dedicated to miniaturisation, improved power handling and excellent electrical performance are still of great significance.

Of particular importance to modern filter design is not only excellent electrical performance, but also size and volume. Since the performance of a filter is highly dependent on its electrical size (expressed as a fraction of its operational wavelength) it comes as no surprise that filters operating at the lower end of the frequency spectrum are physically large. This is of particular concern to telecommunications equipment suppliers. Coaxial cavity filters [1] remain most often used filtering devices in traditional communication networks, due to their excellent technological maturity, cost effectiveness and performance [1]–[8]. Their dominance in the telecommunications industry is marred only by their size and weight, which is often traded on the account of reduced electrical performance. Capacitive loading [9] and a stepped

resonant post [10], [11] are often deployed to reduce resonator profile, albeit at the expense of performance. Helical resonators, [12]–[14] can also be used to address the issue of bulky size.

A space saving approach proposed in [15], [16] relies on the sharing of a resonant cavity by two resonant posts operating at distinct frequencies. Even though this configuration offers good performance, the major limiting factor lies with the large and necessary frequency separation between the resonant frequencies of the resonant posts, so as to maintain a low mutual coupling level. Another type of low-profile coaxial cavity filters was considered in [17]. The proposed resonator consists of a cavity enclosure and two metallic cylinders protruding the cavity from the opposite sides and forming a capacitance in the mutually overlapping area. An additional benefit of the proposed technology is a superior spurious free-response. However, miniaturization potential of such resonator is limited due to its fundamental principles of operation.

Recently a new class of cavity resonators and filters, termed distributed resonators [18], was introduced. The distributed resonator allows a major reduction in the resonator profile while maintaining an excellent electrical performance. In [18], an individual distributed resonator consists of a

The associate editor coordinating the review of this manuscript and approving it for publication was Wenjie Feng.

number of low-profile resonant posts arranged in a grid, where the resonant posts on the vertical and horizontal axes of the grid mainly couple to their immediate neighbours. The substantial reduction in the filter profile, comes – to a degree – at the price of the footprint, mainly due to the fact that the individual distributed resonator consists of a number of resonant posts.

In our previous contribution of [19], the concept of [18] is somewhat further generalized, where it was suggested that a resonant element of [18] can itself be made in a distributed form. Here, we fully build upon the ideas of [19], to provide a detailed theoretical study of the new resonator and access its key performance indicators. The new resonator is named split-distributed resonator, so as to emphasise the fact that the individual resonant post is physically split in order to increase mutual coupling among the resonant posts. The major gain of this new configuration lies with the fact the resulting resonant posts not only couple along the horizontal and vertical axes, but along the respective diagonals too. This results in a more uniform distribution of the electrical fields within the cavity, which demonstrates through the reduction of the resonator footprint, while retaining excellent electrical performance. In order to practically demonstrate the strength of this configuration, two filters have been manufactured, tested and benchmarked against the predicted computed responses.

II. THEORY AND ANALYSIS

A. STUDY OF SPLIT-DISTRIBUTED RESONATOR

A 3-by-3 distributed resonator, as introduced in [18] is shown in Fig. 1. The complete distributed resonator consists of 9 individual, inter-digitated resonant elements arranged in a grid configuration. The inter-digitated configuration allows for a greater level of coupling among the immediate resonant elements on the horizontal and vertical axes of the grid. The resonant elements on the diagonal axes couple relatively weakly. This is primarily due to the fact that the gap among the horizontal and vertical resonant elements is smaller than the gap among the diagonal elements and, also, because the coupling between resonant elements emanating from the same side of the ground plane is smaller compared to the inter-digitated configuration. For the purpose of fully utilising the potential of [18], the level of mutual coupling among the resonant elements needs to be increased. This is achieved by the resonator in Fig. 2. To be specific, each resonant element of Fig. 2 is now split so as to form a distributed resonator itself. The individual resonant element of this figure can now be thought of as a distributed resonant element of the fourth order. In order to permit ease of identification of these new resonators, it is adopted for them to be referred to as $R_{n,m}$ resonator, where n stands for the order of the individual distributed resonator element, and m stands for the number of such distributed resonant elements in a resonant chamber. Using the proposed nomenclature, the resonator of Fig. 2 can be referred to as $R_{4,9}$.

It is now instructive to study the input admittance of a split-distributed resonator designated as $R_{n,4}$, where n is allowed

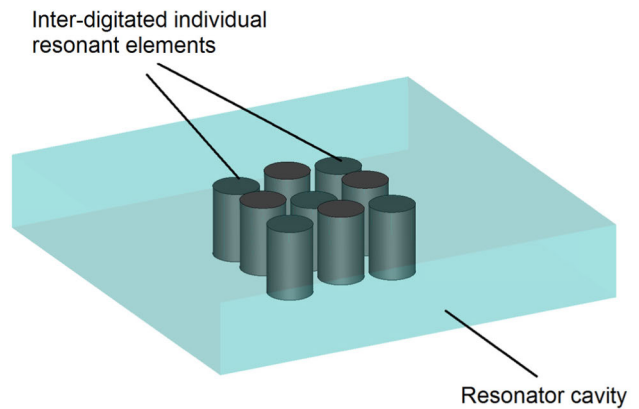


FIGURE 1. Perspective view of 3-by-3 distributed resonator.

to attain an arbitrary value. As an example, an equivalent circuit of Fig. 3 is used. Here, Y_{ij} , $i, j = 1, 2$ represent the admittances of the individual distributed resonant elements, while $Y_{h,i1}$, $i = 1, 2$ and $Y_{v,1j}$, $j = 1, 2$ denote the respective admittance transformers in the horizontal and vertical directions. The admittance transformer, $Y_{c,12}$, stands for the coupling between the top-left to bottom-right diagonal resonant elements Y_{11} and Y_{22} while the coupling between the down-right to top-left diagonal elements, Y_{12} and Y_{21} , can be neglected. In order to understand the reasons for this, one needs to appreciate that all resonant elements of an exemplary split-distributed resonator of Fig. 2 (a) are distributed resonant elements of the second order, i.e., each of them consists of two mutually coupled individual resonant elements. Let us denote the individual resonant elements of the distributed resonant element Y_{12} as R_{12} and L_{12} and the individual resonant elements of the distributed resonant element Y_{21} as L_{21} and R_{21} . In this designation, L and R stand for left and right, respectively. The coupling between Y_{21} and Y_{12} elements occurs, effectively through the coupling of R_{21} and L_{12} . With reference to Fig. 2 (a), these elements have a very small surface area through which they can couple to each other, compared to elements Y_{11} and Y_{22} and can therefore be neglected.

The resonant frequencies of the equivalent circuit of Fig. 3 can be found from the condition that the input admittance is zero. The final analytical formula of the input admittance can be greatly simplified if the following is assumed:

1. All distributed resonant elements are the same, i.e., $Y_{ij} = Y_0$, $i, j = 1, 2$.
2. Admittance transformers connecting the distributed resonant $Y_{h,i1}$, $i = 1, 2$ and $Y_{v,1i}$, $i = 1, 2$ are identical, i.e., $Y_{h,i1} = Y_{v,1i} = Y_t$, $i = 1, 2$.

This yields the following:

$$Y_{in} = Y_0 + \frac{Y_t^2}{Y_0} + 2 \frac{Y_t^2}{Y_0 + \frac{Y_t^2(C+2)}{Y_0}} \quad (1)$$

In (1), C represents the amount of the coupling that exists between the diagonal elements Y_{11} and Y_{22} expressed as a portion of the coupling that exists among the horizontal and vertical distributed resonant elements, Y_t , i.e.,

$$C = \frac{Y_{c,12}}{Y_t} \tag{2}$$

where $Y_{c,12}$ is the characteristic admittance of the transformer connecting the diagonal elements Y_{11} and Y_{22} . Setting (1) to 0, yields the resonant conditions to be imposed on Y_0 ,

$$Y_{0,1,2,3,4} = \pm Y_t \sqrt{\frac{-(C^2 + 3C + 4) \pm \sqrt{C^4 + 2C^3 + C^2 + 8C + 16}}{2}} \tag{3}$$

The resonant frequencies obtained using (3) strongly depend on the physical realization of the admittance, Y_0 , i.e. the order of the split distributed resonator. Further, it can be shown that $Y_{0,1,2,3,4}$ is always imaginary and, therefore can be represented as

$$Y_{0,1,2,3,4} = jB_{0,1,2,3,4} \tag{4}$$

where $B_{0,1,2,3,4}$ represents the susceptance of $Y_{0,1,2,3,4}$. Depending on the realization of the individual distributed resonant element, several cases can be distinguished.

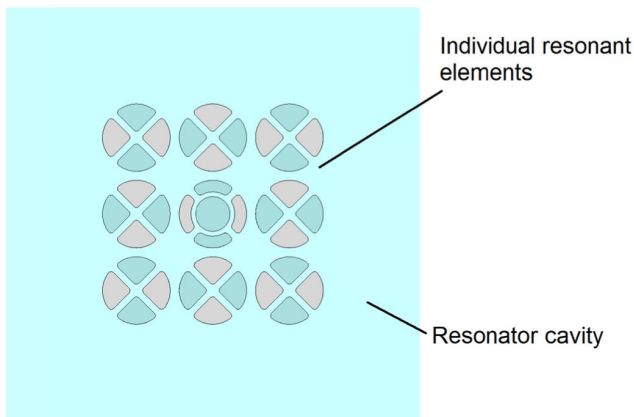


FIGURE 2. Top view of $R_{4,9}$ split-distributed resonator.

A.1 CASE OF Y_0 REALIZED USING FIRST ORDER DISTRIBUTED RESONANT ELEMENTS

This case corresponds to the classical distributed resonator of [18]. It is obtained by setting C in (1) to zero, to yield the well-known relation for the input admittance

$$Y_{in} = Y_0 + 2 \frac{Y_t^2}{Y_0 + \frac{2Y_t^2}{Y_0}} \tag{5}$$

where $Y_0 = Y_{ind} = j\omega C_0 + \frac{1}{j\omega L_0}$. Here, ω stands for the angular frequency of operation, while C_0 and L_0 represent

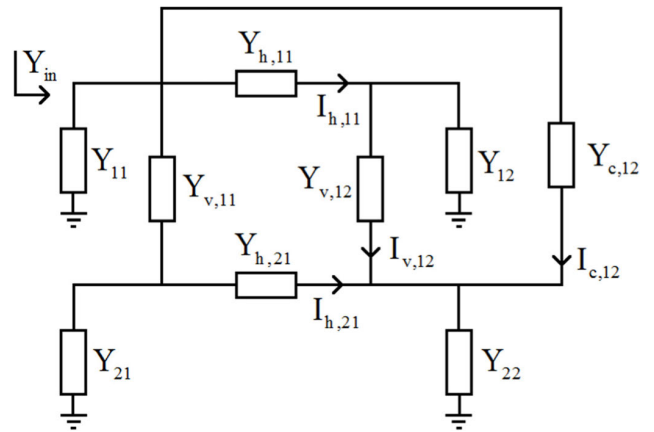


FIGURE 3. Equivalent circuit of split-distributed resonator, $R_{2,4}$.

the equivalent capacitance and inductance of a distributed resonant element. Setting (5) to zero, one obtains its resonant frequencies,

$$\omega_1 = \frac{\sqrt{2C_0 + 4Y_t^2 L_0 + 4Y_t \sqrt{Y_t^2 L_0^2 + L_0 C_0}}}{C_0 \sqrt{2L_0}} \tag{6a}$$

$$\omega_2 = \frac{\sqrt{2C_0 + 4Y_t^2 L_0 - 4Y_t \sqrt{Y_t^2 L_0^2 + L_0 C_0}}}{C_0 \sqrt{2L_0}} \tag{6b}$$

It can be shown that ω_2 is always lower than ω_1 and, as such, it is of importance to the realization of miniaturized resonators.

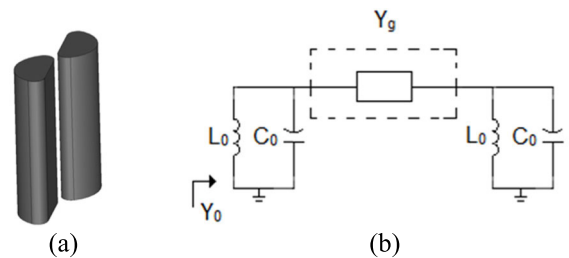


FIGURE 4. Individual distributed resonant element of second order (a) and its equivalent electrical circuit (b).

A.2 CASE OF Y_0 REALIZED USING SECOND ORDER DISTRIBUTED RESONANT ELEMENTS

The individual resonant element in this case is a distributed resonant element of the second order, shown in Fig. 4 (a), and its equivalent circuit is shown in Fig. 4 (b). This case is equivalent to splitting a first order resonant element in two halves along the z -axis. The input admittance of the circuit of Fig. 4 (b) is then

$$Y_0 = Y_{ind} + \frac{Y_g^2}{Y_{ind}} \tag{7}$$

where, as before, $Y_{ind} = j\omega C_0 + \frac{1}{j\omega L_0}$. Here, ω stands for the angular frequency of operation, while C_0 and L_0 represent the equivalent capacitance and inductance of a single element of the distributed resonant element of the second order. Here, it was assumed that the constituent elements of the distributed resonant element have identical inductances and capacitances. Y_g stands for the admittance transformer, representing the coupling between the two constituent elements. It is now instructive to define Y_g in terms of the admittance transformer (coupling) among the individual distributed elements Y_t of Fig. 3 in the following fashion

$$K = \frac{Y_g}{Y_t} \tag{8}$$

Substitution of (8) and (7) into (4) yields a set of 4 polynomial equations of the fourth order, resulting in 16 roots.

$$\begin{aligned} \omega^4 (L_0^2 C_0^2) - \omega^3 (B_{0,i} L_0^2 C_0) - \omega^2 (2L_0 C_0 + K^2 Y_t^2 L_0^2) \\ + \omega (B_{0,i} L_0) + 1 = 0 \end{aligned} \tag{9}$$

for $i = 1, 2, 3, 4$

(9) yields 16 roots in total. Half of the roots have negative real values, while the remaining 8 roots have positive real values. Since negative roots are not physically possible, only the positive roots are of importance. For the purpose of the proposed split-distributed resonator, the minimum-value root is of most importance.

A.3 CASE OF Y_0 REALIZED USING FOURTH ORDER DISTRIBUTED RESONANT ELEMENTS

In this case is a distributed resonant element of the fourth order, as shown in Fig. 5 (a). This case is equivalent to splitting a first order resonant element in four quarters along the z-axis. The equivalent circuit of this resonator is presented in Fig. 5(b). Here, it can be assumed that the coupling between the opposing resonant elements is negligible and that it can be ignored. This figure also shows that the resonant element on the right-hand side is load-pulled by its two immediate neighbouring elements, resulting in a decrease in the admittance “seen” from their side. The decrease in this admittance is reflected in the increase of the inductance and the reduction in the capacitance of the stand-alone resonant element, shown in Fig. 5 (c). From this figure, the expression for the input admittance, Y_0 , can be written as

$$Y_0 = Y_{ind} + \frac{2Y_g^2}{Y_{ind} + \frac{Y_g^2}{\left(\frac{Y_{ind}}{2}\right)}} \tag{10}$$

where, as in the previous section, $Y_{ind} = j\omega C_0 + \frac{1}{j\omega L_0}$. Substituting the expression for Y_{ind} into (10) and equating the final expression into (4), one obtains a set of 4 sixth order polynomial equations,

$$A_1 \omega^6 + A_2 \omega^5 + A_3 \omega^4 + A_4 \omega^3 + A_5 \omega^2 + A_6 \omega + 1 = 0 \tag{11}$$

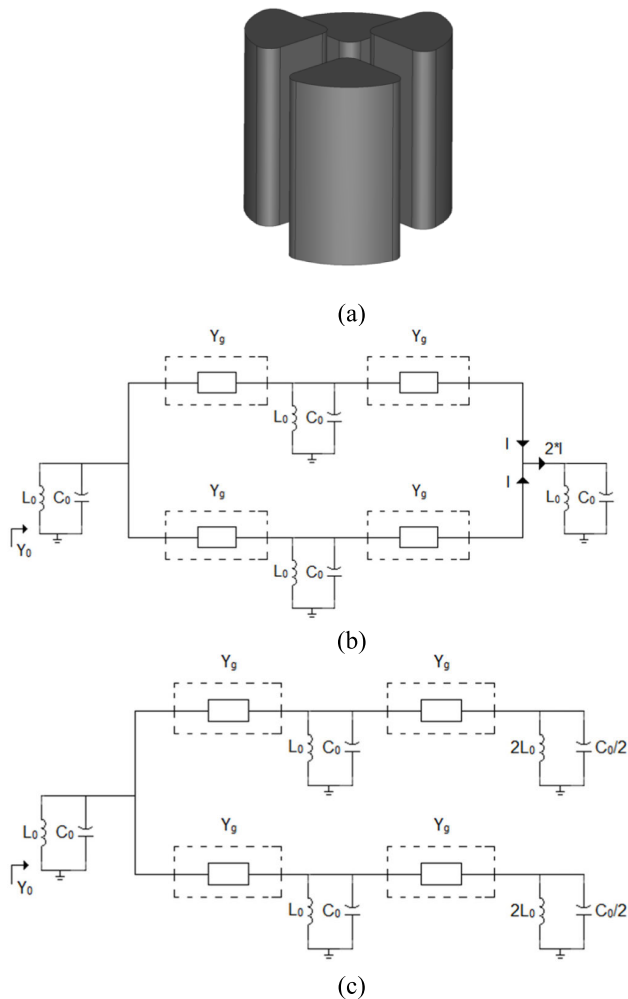


FIGURE 5. Individual distributed resonant element of fourth order (a), its equivalent electrical circuit with load-pulling shown (b) and with load pulling taken into account (c).

where $A_1 = -L_0^3 C_0^3$, $A_2 = B_{0,i} L_0^3 C_0^2$, $A_3 = 3L_0^2 C_0^2 + 4K^2 Y_t^2 L_0^3 C_0$, $A_4 = -2B_{0,i} L_0^2 C_0 - 2B_{0,i} K^2 Y_t^2 L_0^3$, $A_5 = -3L_0 C_0 - 4K^2 Y_t^2 L_0^2$ and $A_6 = B_{0,i} L_0$.

As in the previous case, half of the roots of (11) are negative and need to be discarded as non-physical. Out of the remaining positive 12 roots, the minimum value root is of most importance for the purpose of filter miniaturization.

A.4 CASE OF Y_0 REALIZED USING ARBITRARY n-ORDER DISTRIBUTED RESONANT ELEMENTS

The equivalent circuits of the distributed resonant elements of an arbitrary, n-th order is shown in Fig. 6. The input admittance can be written as

$$Y_0 = Y_{ind} + \frac{2Y_g^2}{Y_{ind} + \frac{Y_g^2}{Y_{ind} + \dots + \frac{Y_g^2}{\left(\frac{Y_{ind}}{2}\right)}}} \tag{12}$$

By equating (12) to (4), a set of 4, polynomial equations of the $n+2$ order are obtained. As in the previous cases, there are $2(n+2)$ negative and $2(n+2)$ positive roots. Again, the root of most importance is the minimum value positive root.

It is now instructive to compare the performance of the 2 distributed resonators proposed in [18] for the same spacing of proposed $R_{n,4}$ split-distributed resonator with a standard 2-by-2 resonant elements. For this purpose, only the lowest frequencies of operation of all resonators are of interest and need to be plotted against the impedance transformer common to both resonators, given by $Z_t = \frac{1}{Y_t}$. This, however, necessitates the knowledge of the values of C in (2) and K in (8).

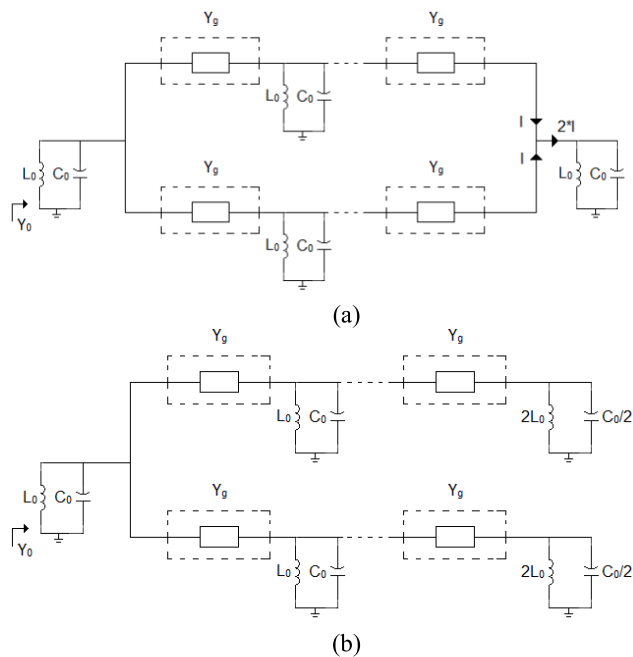


FIGURE 6. Equivalent electrical circuit of individual distributed resonant element of n -th order with load-pulling shown (a) and with load pulling taken into account (b).

Selection of the values for C and K given by (2) and (4), respectively, requires a somewhat deeper elaboration. With reference to Fig. 2, it can be observed that the inter-distributed element coupling on the horizontal and vertical axes occurs across a shorter separation distance of the distributed resonant elements than its counterpart on the upper-left-to-lower-right diagonal. Furthermore, the inter-distributed coupling on the horizontal and vertical axes takes place through a considerably smaller surface area than the inter-distributed coupling along the upper-left-to-lower-right diagonal. These two means of coupling are in opposition to each other – in other words, coupling between any elements is indirectly proportional to the physical separation of the elements and directly proportional to the surface areas through which the elements couple. In view of this, C given by (2) is likely to attain values smaller than 1. In a similar manner, intra-distributed element coupling occurs across a large surface area than the inter-distributed element coupling on the vertical and horizontal axes. This infers that intra-distributed

element coupling – hence the admittance transformer Y_g – is always greater or equal to the equivalent admittance transformer of the inter-distributed element coupling, Y_t . This, in turn, makes K given by (8) always greater or equal to 1. It is now instructive to examine the lowest resonant frequencies of the proposed split-distributed resonators, $R_{2,4}$, and $R_{4,4}$ for different values of C and K and compare the frequencies with the lowest operating frequency of the standard, 2-by-2, distributed resonator for the same levels of inter-distributed element coupling. The individual resonant elements in both cases are assumed to operate at the same frequency of 2 GHz. The comparison of the lowest frequencies of operation is shown in Fig. 7 for three sets of values for C and K, namely a) C = 0.3 and K = 1, b) C = 0.3 and K = 1.5 and c) C = 0.6 and K = 1.5. The figure indicates that regardless of the values assigned to C and K, the proposed split-distributed resonator always resonates at a frequency that is lower than its standard distributed resonator counterpart. Furthermore, the figure also shows the increase of the order of the individual distributed resonant elements is followed by the reduction in the frequency of operation. The main reason rests with the additional sources of element coupling – the intra-distributed element coupling and the coupling along the upper-left-to-lower-right diagonal. With reference to Fig. 7, the lowest frequency of operation for a strong coupling results in the lowest frequency of operation of the standard distributed resonator of about 905 MHz, whereas the lowest frequency of operation of the proposed $R_{2,4}$ and $R_{4,4}$ resonators takes place when C = 0.6 and K = 1.5 and equals to 723 MHz and 636 MHz, respectively. In percentage terms, this is equivalent to the reduction of the frequency of operation of about 20 % and 30 % compared to the standard distributed resonator, respectively. However, it should be mentioned that there is a limitation of resonant frequency reduction by means of increasing the resonator order, which, mathematically, is a consequence of the fact that input admittance, Y_0 , is in the form of a continuous generalized fraction, which has a high rate of convergence as a function of the number of its elements. This is clear from Fig. 7.

Resonant frequencies of higher-orders split-distributed resonators can also be obtained numerically. However, the orders of the corresponding polynomials that need to be solved would be considerably increased. Such high-order polynomials, even though solvable numerically, are cumbersome. From the performance evaluation point of view, it is more appropriate to analyze split-distributed resonators using a full-wave simulator, which will not only reveal the frequencies of operation, but also give an insight into the electrical performance. In the next subsection, the key characteristics of the proposed resonator – namely frequency tunability and achievable coupling bandwidths – are examined.

A.5 STUDY OF KEY PARAMETERS OF SPLIT-DISTRIBUTED RESONATOR

For the purpose of studying frequency tunability and achievable coupling bandwidths, $R_{1,9}$, $R_{2,9}$ and $R_{4,9}$ split-

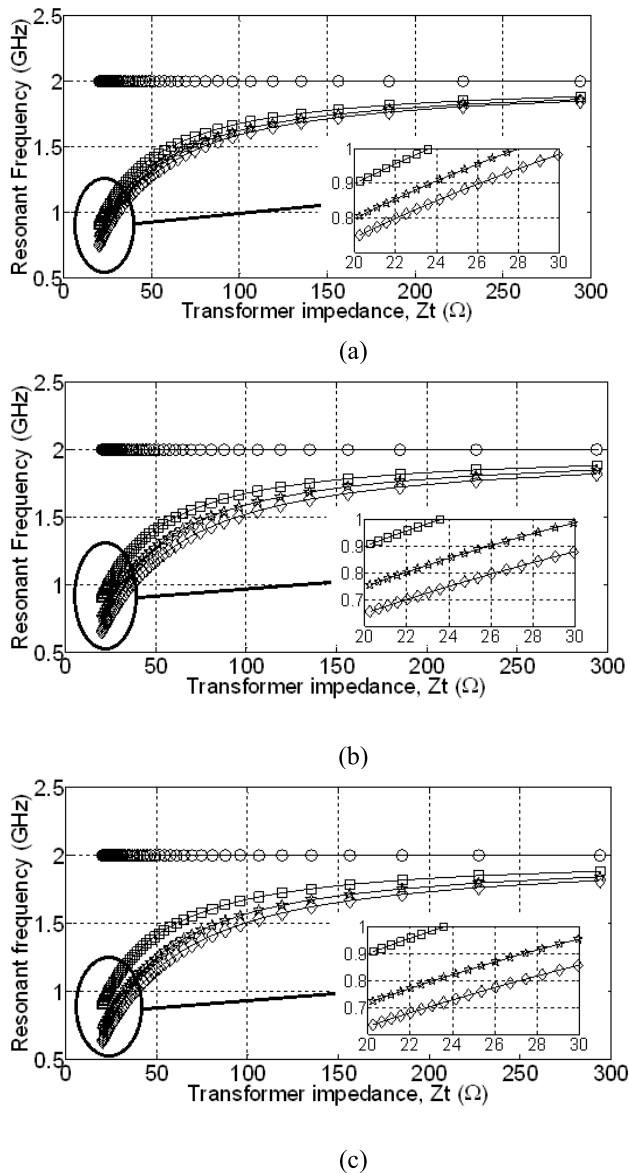


FIGURE 7. Lowest resonant frequencies of resonators as functions of transformer impedance – circles: single resonator; squares: standard 2-by-2 distributed resonator; stars: $R_{2,4}$ split-distributed resonator and diamonds: $R_{4,4}$ split-distributed resonator for a) $C = 0.3$ and $K = 1$, b) $C = 0.3$ and $K = 1.5$ and c) $C = 0.6$ and $K = 1.5$.

distributed resonators consisting of 9 sets of distributed resonant elements arranged in a rectangular, 3-by-3 pair, grid, are considered. The volume occupied by these resonators is $40 \times 40 \times 7 \text{ mm}^3$, $30 \times 30 \times 7 \text{ mm}^3$ and $30 \times 30 \times 5 \text{ mm}^3$, respectively. For illustrative purposes, the $R_{2,9}$ resonator with the indicated dimensions is shown in Fig. 8. With reference to this figure, the distributed resonant element located in the center of the grid is further split to allow the introduction of a tuning screw. The individual resonant elements are of identical radius $\text{Rad} = 2.1 \text{ mm}$, and the radius of the tuning screw is $\text{Rad_middle} = 1.25 \text{ mm}$. All distributed resonant elements have a height of 6.05 mm, which allows for a gap of 0.95 mm between the top of the resonator and the corresponding ground plane. Such a gap can be considered

adequate from the power-handling point of view. The separation between the individual resonant elements, denoted as d_{intra} , is 0.5 mm, and the separation between any two neighboring pairs of distributed elements is $d_{\text{inter}} = 0.85 \text{ mm}$. These values have been obtained by considering the goal of achieving an equal distribution of the electric field intensity among all elements of the proposed distributed resonator. The radii, heights, intra and inter gaps are the same for the remaining two split-distributed resonators, $R_{1,9}$ and $R_{4,9}$.

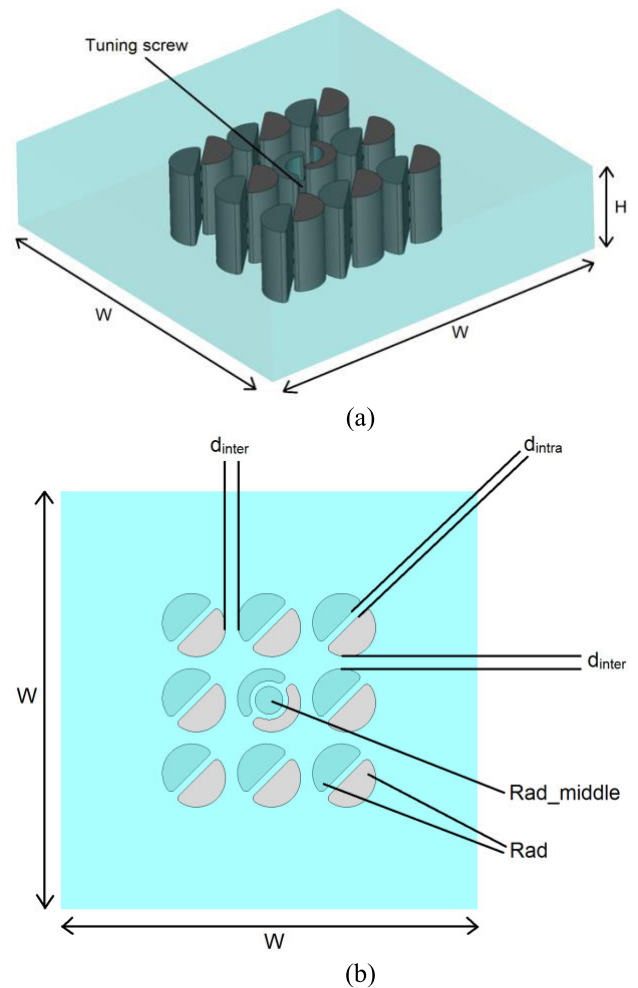


FIGURE 8. Split-distributed resonator, $R_{2,9}$ – (a) perspective view; (b) top view.

Frequency tunability of these resonators as a function of the tuning screw intrusion into the cavity is shown in Fig. 9. In the case of the $R_{1,9}$ and $R_{2,9}$ resonators, the tuning screw is allowed to intrude into the cavity by up to 6.5 mm, leaving a minimum gap between the head of the tuning screw and ground plane of 0.5 mm. Similarly, for the case of the $R_{4,9}$ resonator, the tuning screw is allowed to protrude the cavity up to 4.5 mm, leaving a minimum gap of 0.5 mm. The results presented in this figure indicate that frequency tunabilities of 156 MHz, 82 MHz and 44 MHz have been achieved for the $R_{1,9}$, $R_{2,9}$ and $R_{4,9}$ resonators, respectively. This result does not come as a surprise, since the increase in the number

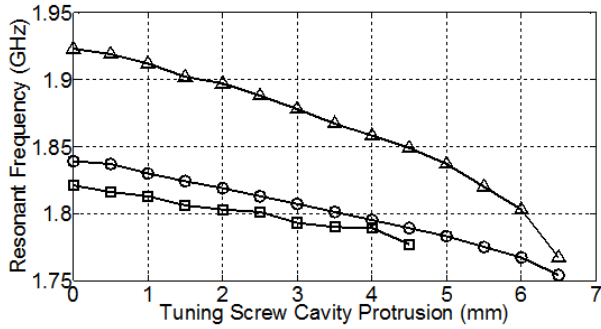


FIGURE 9. Resonant frequency of $R_{1,9}$ (triangles), $R_{2,9}$ (circles) and $R_{4,9}$ (squares) split-distributed resonator as a function of tuning screw intrusion.

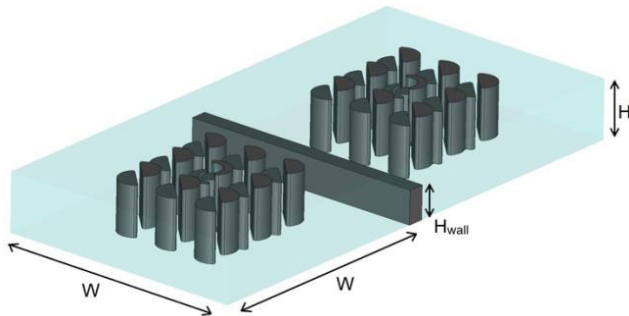


FIGURE 10. Two split-distributed resonator structure used in study of coupling bandwidth.

of individual resonant elements results in a relative frequency insensitivity.

Next, the coupling coefficient of the proposed resonators is studied. For this purpose, a two-resonator structure of Fig. 10, is used. The figure depicts two $R_{2,9}$ resonators separated by a conductive wall, however, for the purpose of this study coupling was also investigated for the cases when the individual resonators are $R_{1,9}$ and $R_{4,9}$. In this investigation, each individual split-distributed resonator is made to operate, in a stand-alone configuration, at a frequency of 1.8 GHz, by protruding the tuning screw into the cavity by an appropriate length: 6mm, 3.5 mm and 2 mm for the $R_{1,9}$, $R_{2,9}$ and $R_{4,9}$ resonators, respectively. The coupling coefficient of this structure as a function of the separation wall height, H_{wall} , is given in Fig. 11. This figure indicates that the maximum coupling coefficient is achievable with the $R_{4,9}$ resonator.

III. RESULTS

For further investigation of the split-distributed resonators, four 5-pole individual resonators of different order operating at the same frequency 1.8 GHz are simulated and analyzed. Table 1 presents the details of the considered resonators. The respective resonators of Table 1 are shown in Fig. 12, while their performance was by means of a 3D numerical simulator, CST Studio Suite (2018), employing the same numerical settings. In the simulations, it was assumed that all metal parts of the cavities have a conductivity that is about 15% lower than that of pure silver, in order to account for possible silver impurities and other fabrication-related defects.

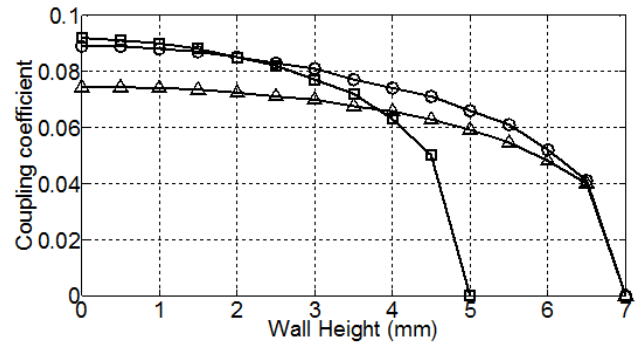


FIGURE 11. Actual coupling coefficient of $R_{1,9}$ (triangles), $R_{2,9}$ (circles) and $R_{4,9}$ (squares) split-distributed resonator as functions of separation wall height of structure of FIGURE 10.

Table 1 indicates that the unloaded Q-factor over volume is steadily increases at first and then saturates as the number of individual resonant elements is increased, for the case of the identical resonant frequencies. It is worth noting that, Q_u/V of the four examined resonators is increased from 0.21 for the case of a standard distributed resonator to the value of 0.3 for the case of the $R_{4,9}$ and $R_{8,9}$ split-distributed resonators. For comparison, a standard single resonant post resonator is also included in the table.

In order to validate the proposed theory on the split-distributed resonators, two 5-pole Chebyshev filters based on $R_{4,9}$ and $R_{2,9}$ resonators and operating at 1.8 GHz are designed and fabricated. We do not consider split-distributed resonator $R_{8,9}$ since its electrical performance is very similar to the $R_{4,9}$ resonator. However, its fabrication is expected to be rather challenging, due to the small size of the constituent resonant elements.

The two 5-pole filters have been designed for a minimum return loss of 16 dB and a percentage bandwidth of about 2.2 %. Their coupling matrices are identical and are given by

$$M = \begin{pmatrix} 0 & 0.01755 & 0 & 0 & 0 \\ 0.01755 & 0 & 0.01344 & 0 & 0 \\ 0 & 0.01344 & 0 & 0.01344 & 0 \\ 0 & 0 & 0.01344 & 0 & 0.01755 \\ 0 & 0 & 0 & 0.01755 & 0 \end{pmatrix} \quad (13)$$

In the next subsections, the performances of the fabricated filters will be shown and compared to their performance obtained by simulations.

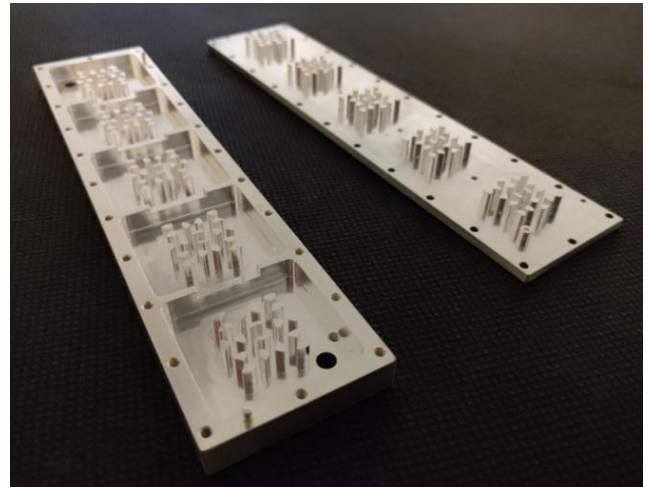
A.1 5-POLE FILTER USING $R_{4,9}$ RESONATORS

The fabricated filter using $R_{4,9}$ resonators operating at a centre frequency of 1.8 GHz is shown in Fig. 12. Its internal dimensions are $158 \times 30 \times 5 \text{ mm}^3$. The entire filter consists of two parts – bottom and top which are held together with 24 M2 screws, appropriately torqued to the value of 1 N·m. The widths of the filter walls are 4 mm.

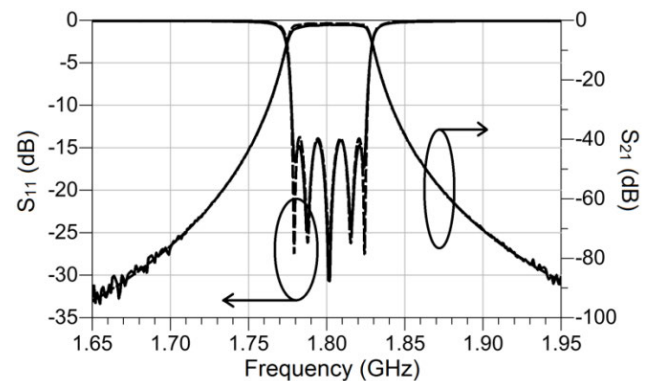
The coupling between the consecutive resonators is obtained using irises, while the input/output coupling is obtained using a grounded conductive pin placed in the

TABLE 1. Performance Comparison of Standard, 3-by-3, Distributed Resonator of [18] and Split-Distributed, $R_{2,9}$, Resonator.

	Resonant frequency [GHz]	Q_u factor	Volume [mm ³]	Maximum electric field intensity $\times 10^9$ [V/m]	Q_u/V	Q_u (perfect silver)
Standard distribute, 3-by-3 resonator [18]	1.8	2380	40x40x7	2.69	0.21	2578
$R_{2,9}$ resonator	1.8	1790	30x30x7	2.67	0.28	1933
$R_{4,9}$ resonator	1.8	1375	30x30x5	2.61	0.3	1485
$R_{8,9}$ resonator	1.8	1218	30x30x4.5	2.45	0.3	1315
Single res. post resonator	5.653	4072	30x30x5	4.63	0.9	4398

**FIGURE 12. Fabricated 5-pole split-distributed filter using $R_{4,9}$ operating at 1.8 GHz.**

vicinity of the first resonant element. Its physical separation from the first resonant element dictates the coupling bandwidth. The response of the filter is shown in Fig. 13, while an exploded view of the passband is shown in Fig. 14. The measured return loss is somewhat lower (less than 2 dB) compared to its computed value. The measured insertion loss is about 1.4 dB, which is higher than the value of 1 dB, predicted by the simulations. The discrepancy of 0.4 dB, which is equivalent to the reduction of the unloaded Q of about 32 %, cannot be entirely attributed to the manufacturing imperfections, such as silver impurities and surface roughness. Silver plating impurities together with surface roughness are, industrially expected, to deteriorate the unloaded Q factor by approximately 10-15%. Therefore, the difference between the observed discrepancy (32 %) and the expected discrepancy (10-15%) of between 17-22% points to a new source of deleterious influence. It is well known in the industry that an imperfect ground contact leads to a reduction in the unloaded Q factor. In order to test if the imperfect contact between the two filter plates of Fig. 12 is the source of deterioration, the unloaded Q factor of a single cavity was measured as a function of the applied pressure between the two plates. Initially, the screws used to hold the two plates together were torqued to the value of 1 N·m and the achieved unloaded Q factor was measured. Then, the device was placed in a controlled pressure environment, where pressure was applied to the top and bottom parts of the cavity. The unloaded Q factor was measured as a function of the applied pressure. For clarity, the measured values of the applied pressure were recalculated to the equivalent values of the tightening torque for M2 screws. This was done using the procedure described in [20] and assuming that the friction coefficient of silver-plated screws is about 0.4. Table 2 shows the measured results. This table shows that the measured Q factor monotonically increases and then saturates as a function of the applied pressure. The initial value of the Q factor with no pressure applied is 922, which saturates to the value of 1149 at a pressure level of 10 tsi. The discrepancy between the simulated Q factor of 1360 and the measured Q factor at a pressure level of 10 tsi

**FIGURE 13. Measured and simulated responses of 5-pole split-distributed filter of FIGURE 12 – dashed line: computed; solid line: measured.**

of 1149 is about 15%, reduced from the level of about 32%. The 15 % difference between the measured and simulated Q factors forms the upper acceptance limit for the discrepancies attributable to silver impurities and manufacturing imperfections. It is, hence, probable that an additional mechanism responsible for the degradation of performance is present. However, based on the available results, such a contributor is expected to mildly influence performance degradation. By way of the elimination of the least possible and least likely causes, the relative uncertainty in the spatial position of the resonant elements on the top and bottom parts of the filter may be the additional, minor contributor to the degradation of the unloaded Q factor. However, this is difficult to verify in practice, due to the inaccessibility to the resonant elements once the two filter parts are screwed together.

The group delay and the wideband transmission coefficient are shown in Figs. 15 and 16. The measured and predicted delay values are in an excellent agreement, while the wideband performance indicates that the first spurious response occurs at approximately 3.52 GHz. The spurious responses are due to cavity resonances. In particular, the first two cavity modes propagate along the x and y axis, respectively, and exhibit a similar propagation environment, which is reflected

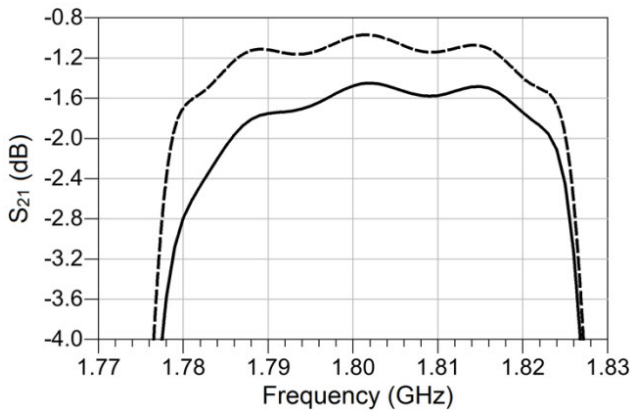


FIGURE 14. Magnified view of passband of the filter's response of FIGURE 13.

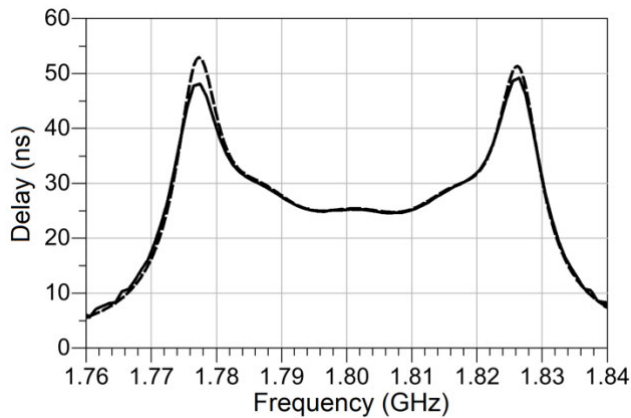


FIGURE 15. Group delay of filter of FIGURE 12 – dashed line: computed; solid line: measured.

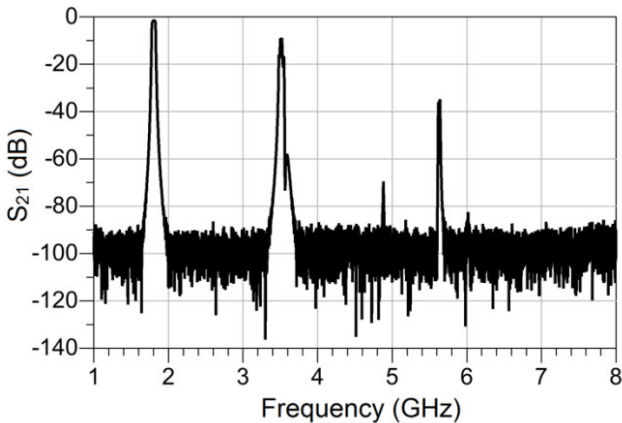


FIGURE 16. Measured wideband response of filter of FIGURE 12.

in their similar frequencies of operation. The degeneration of these two modes is somewhat disturbed by the slight asymmetry of the $R_{4,9}$ resonator along the x and y axes, resulting in the resonant frequencies of 3.52 GHz and 3.55 GHz for the first and second spurious response, respectively. The fact that the propagation environment inside the cavity is influenced by the arrangement and the mutual proximity of the individual resonant elements, points to a possible way of improving the out-of-band response. For example, this could be done by carefully adjusting the couplings among

TABLE 2. Measured Unloaded Q-factors of Single Cavity of $R_{4,9}$ Resonator at 1.8 GHz.

Pressure [tons per square inch (tsi)]	Equivalent Torque [N·m]	Unloaded Q-factor
0	1	922
2	2	988
3	3	1094
4	4	1129
5	5	1140
6	6	1145
7	7	1146
8	8	1146
9	9	1149
10	10	1149

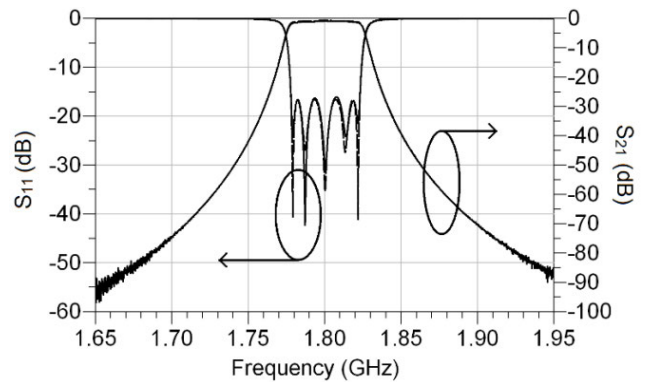


FIGURE 17. Measured and simulated responses of 5-pole split-distributed filter based on $R_{2,9}$ resonators – dashed line: computed; solid line: measured.

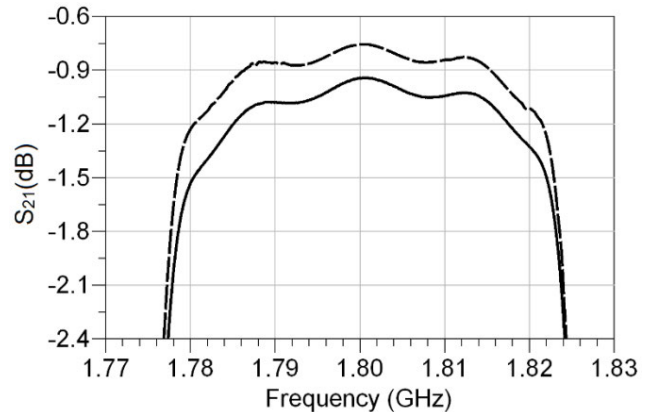


FIGURE 18. Magnified view of passband of 5-pole split-distributed filter based on $R_{2,9}$ resonators.

the resonant elements, or by introducing high frequency short circuits positioned at locations where the electric field at the frequencies of the spurious responses is at a maximum. Of course, care must be taken so that the electric field at the fundamental frequency is minimally disturbed.

A.2 5-POLE FILTER USING $R_{2,9}$ RESONATORS

The measured and simulated responses of the fabricated 5-pole filter based on $R_{2,9}$ resonators are shown in Fig. 17.

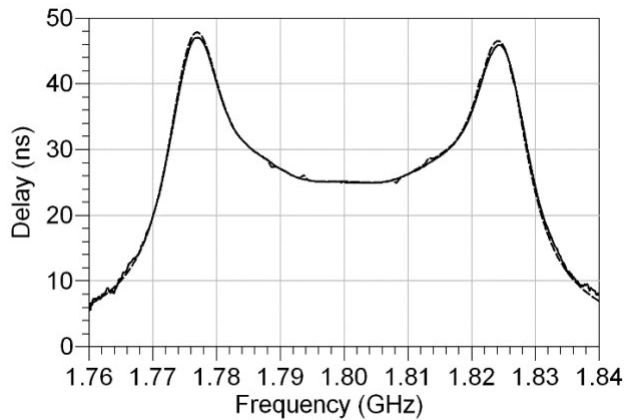


FIGURE 19. Group delay of 5-pole split-distributed filter based on $R_{2,9}$ resonators – dashed line: computed; solid line: measured.

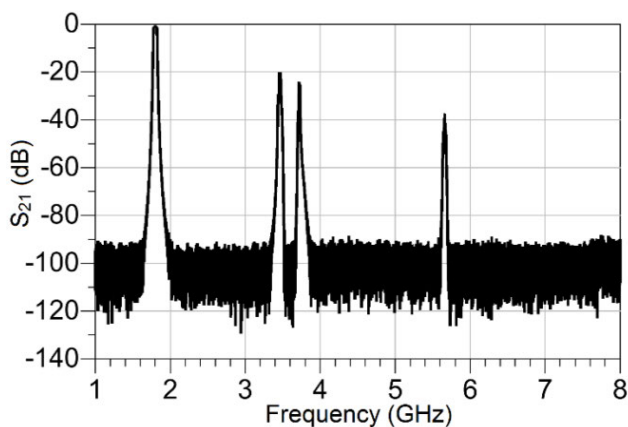


FIGURE 20. Measured wideband response of 5-pole split-distributed filter based on $R_{2,9}$ resonators.

There exists an excellent agreement between the results, evidenced in Fig. 18 which shows an expanded view of the filter's passband. One can appreciate from this figure that the measured insertion loss at the mid-point of the filter's passband of 0.94 dB is contrasted by the value of 0.75 dB predicted by the simulations. The discrepancy can be explained, as in the previous subsection, by the existence of silver impurities, surface roughness and also by the imperfect contact between the two filter plates, Table 2. Fig. 19 depicts a good agreement between the measured and simulated group delays of the filter. The measured wideband response of the fabricated filter is presented as Fig. 20. From this figure, one can infer that the first spurious response occurs at 3.47 GHz, which is about $3.47/1.8 = 1.93$ times greater than the response at the filter's fundamental frequency, which is similar to the case of the filter with $R_{4,9}$ resonators. It is worth noting, however, that the magnitude of this response is about 20 dB lower with respect to the transmission response at the fundamental frequency. Like with the case of $R_{4,9}$ resonators, the spurious response of the $R_{2,9}$ resonators is also due to the cavity. The first two spurious responses are due to the waves propagating diagonally from left to right and from right to left, respectively. Their frequencies of operation are distinct from each other due to the differences in the propagation

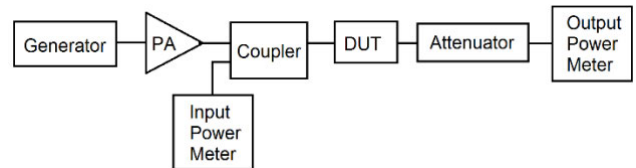


FIGURE 21. Test set-up for high power measurements.

TABLE 3. Power handling capability of proposed filters.

	Resonant frequency [GHz]	Maximum electric field intensity $\times 10^9$ [V/m]	Maximum permissible stored energy [μ J]	Maximum energy stored [nJ] per 1W input	Maximum allowable power [W]
$R_{1,9}$ resonator	1.8	2.69	1.24	19.5	63.6
$R_{2,9}$ resonator	1.8	2.67	1.26	18.9	66.6
$R_{4,9}$ resonator	1.8	2.61	1.32	18.4	71.7

environment. To be exact, the differences in the propagation environment can be attributed to the orientation of the resonant elements, as seen in Fig. 8. The frequencies of the first two spurious modes are 3.47 GHz and 3.74 GHz, respectively, as shown in Fig. 20. Higher order spurious modes are also due to the cavity.

The power handling capability of the fabricated filters is assessed next. From the knowledge of the electric field strength at which dielectric breakdown occurs, it is possible to infer the maximum permissible stored energy inside the fabricated filters. Given the fact that the resonators operate in the air with an electric field strength at breakdown of 3×10^6 V/m, the maximum values of the stored energies inside the resonators are shown in Table 3. Using a commercially available software package [21], which is based on the works of [22] and [23], it is possible to determine the maximum amounts of energy stored in individual filters.

These values are also shown in Table 3. From here and from the calculations of the maximum permissible stored energies, one can infer that the maximum amount of the continuous-wave (CW) power the present filters can handle, Table 3. Also shown in this table is the predicted power handling capability of a standard, 3×3 distributed resonator. In order to test the power handling capability, the manufactured filters were subjected to a power soak test, with the test set-up as shown in Fig. 21. The input power is gradually increased starting from 30 dBm, all the way to 47 dBm (limitations of the equipment) at room temperature. In the conducted tests, no arcing and no changes in the S- parameters were observed up to this maximum power level. Furthermore, no nonlinear dependence of the observed output power as a function of the input power was recorded. This is used as an indication that no nonlinear effects have taken place.

IV. CONCLUSION

A new class of low-profile and low-volume cavity resonators is introduced in this paper. The introduced resonators are named split-distributed resonators, due to the fact that the constituent resonant elements of a standard distributed resonator are themselves realized in a distributed form. In this way, additional couplings among the individual elements are achieved, resulting in a tremendous volume reduction compared to a standard distributed resonator and a more-equalized distribution of the electric field intensity inside the resonator cavity. The distribution of the electric field intensity allows for an excellent electrical and power-handling performance. The required equations describing the operation of the proposed new resonator class are also presented and, based on them, two 5-pole band-pass filters were designed, simulated and fabricated. The measured and simulated responses of the filter are in good agreement.

ACKNOWLEDGMENT

The authors wish to thank Stefan Woerner and Joachim Scherzinger for fabrication of the filters, Leroy Plymale and Doug Pervere for their support with high power measurements, and Nick Jeffers for his consultancy regarding torque measurements.

REFERENCES

- [1] S. B. Cohn, "Direct-coupled-resonator filters," *Proc. IRE*, vol. 45, no. 2, pp. 187–196, Feb. 1957.
- [2] G. L. Matthaei, "Comb-line band-pass filters of narrow or moderate bandwidth," *Microw. J.*, vol. 6, pp. 82–91, Aug. 1963.
- [3] L. Young, "Direct-coupled cavity filters for wide and narrow bandwidths," *IEEE Trans. Microwave Theory Techn.*, vol. 11, no. 3, pp. 162–178, May 1963.
- [4] R. M. Kurzrok, "Design of comb-line band-pass filters," *IEEE Trans. Microw. Theory Techn.*, vol. 14, no. 7, pp. 351–353, Jul. 1966.
- [5] R. Levy, "Theory of direct-coupled-cavity filters," *IEEE Trans. Microwave Theory Techn.*, vol. MTT-15, no. 6, pp. 340–341, Jun. 1967.
- [6] E. G. Cristal, "Tapped-line coupled transmission lines with applications to interdigital and combline filters," *IEEE Trans. Microwave Theory Techn.*, vol. 23, no. 12, pp. 1007–1012, Dec. 1975.
- [7] A. Abramovicz, "Modelling of wide band combline and interdigital filters," in *IEEE MTT-S Int. Microw. Symp. Dig.*, 2010, vol. 16, no. 1, pp. 15–22.
- [8] R. R. Mansour, "Filter technologies for wireless base stations," *IEEE Microwave Mag.*, vol. 5, no. 1, pp. 68–74, Mar. 2004.
- [9] J. B. Thomas, "Cross-coupling in coaxial cavity filters—a tutorial overview," *IEEE Trans. Microwave Theory Techn.*, vol. 51, no. 4, pp. 1368–1376, Apr. 2003.
- [10] S. Yamashita and M. Makimoto, "Miniaturized coaxial resonator partially loaded with high-dielectric-constant microwave ceramics," *IEEE Trans. Microwave Theory Techn.*, vol. 31, no. 9, pp. 697–703, Sep. 1983.
- [11] H. Yao, A. K. Zaki, A. E. Atia, and T. Dolan, "Improvement of spurious performance of combline filters," in *Proc. IEEE Microw. Theory Techn. Symp.*, Denver, CO, USA, Jun. 1997, pp. 1099–1102.
- [12] S. J. Fiedziuszko and R. S. Kwok, "Novel helical resonator filter structures," in *IEEE MTT-S Int. Microw. Symp. Dig.*, Jun. 1998, pp. 1323–1326.
- [13] E. Doumanis, G. Goussetis, W. Steffe, D. Maiarelli, and S. A. Kosmopoulos, "Helical resonator filters with improved power handling capabilities for space applications," *IEEE Microwave Wireless Compon. Lett.*, vol. 20, no. 11, pp. 598–600, Nov. 2010.
- [14] G. Salza, G. Goussetis, C. Vicente, M. Reglero, M. Taroncher, V. Boria, N. Sidiropoulos, J. Galdeano, M. Guglielmi, E. Doumanis, and S. Kosmopoulos, "Helical resonator with modulated radius for improved multipactor threshold: Numerical and experimental results," in *Proc. 46th Eur. Microw. Conf. (EuMC)*, Oct. 2016, pp. 233–236.
- [15] X. Liu, L. P. B. Katehi, and D. Peroulis, "Novel dual-band microwave filter using dual-capacitively-loaded cavity resonators," *IEEE Microwave Wireless Compon. Lett.*, vol. 20, no. 11, pp. 610–612, Nov. 2010.
- [16] M. Jiang, L.-M. Chang, and A. Chin, "Design of dual-passband microstrip bandpass filters with multi-spurious suppression," *IEEE Microwave Wireless Compon. Lett.*, vol. 20, no. 4, pp. 199–201, Apr. 2010.
- [17] E. Doumanis, S. Bulja, and D. Kozlov, "Compact coaxial filters for BTS applications," *IEEE Microwave Wireless Compon. Lett.*, vol. 27, no. 12, pp. 1077–1079, Dec. 2017.
- [18] S. Bulja and M. Gimersky, "Low-profile distributed cavity resonators and filters," *IEEE Trans. Microwave Theory Techn.*, vol. 65, no. 10, pp. 3769–3779, Oct. 2017.
- [19] S. Bulja and D. Kozlov, "Split-distributed resonators and filters," in *Proc. IEEE Radio Wireless Symp. (RWS)*, Orlando, FL, USA, Jan. 2019, pp. 1–3.
- [20] J. Arumala, R. McCulley, and E. Yilmaz, "The relationship between the tightening torque and the clamp force of small industrial screw fasteners," Univ. Maryland Eastern Shore, Princess Anne, MD, USA, Tech. Rep., 2000, doi: 10.18260/1-2-8660.
- [21] (2018). *Guided Wave Technology*. [Online]. Available: <https://www.gwtsoft.com>
- [22] A. Sivasdas, M. Yu, and R. Cameron, "A simplified analysis for high power microwave bandpass filter structures," in *IEEE MTT-S Int. Microw. Symp. Dig.*, Boston, MA, USA, vol. 3, Jun. 2000, pp. 1771–1774.
- [23] C. Wang and K. A. Zaki, "Analysis of power handling capacity of band pass filters," in *IEEE MTT-S Int. Microw. Symp. Dig.*, Phoenix, AZ, USA, vol. 3, May 2001, pp. 1611–1614.



SENAD BULJA (Senior Member, IEEE) received the B.Eng. (Hons.) and Ph.D. degrees from the University of Essex, Colchester, U.K., in 2002 and 2007, respectively.

From 2007 to 2010, he was a Senior Research Officer with the School of Computer Science and Electronic Engineering, University of Essex, where he led the characterization effort of liquid crystals at microwave and millimeter-wave frequencies, and the development of liquid-crystal-based millimeter-wave devices. Since 2010, he has been with Nokia Bell Labs, where he is currently a Senior Research Scientist. He led the research effort in the research and development of low-profile resonators and filters and the discovery of dielectric tunability of inorganic electro-chromic materials and RF switching capability of transition metal oxides. He is also the CTO and Founder of a Nokia spin-out, ArqKos, which focuses on high RF performance filters. He has authored/coauthored over 70 papers in international journals and conference proceedings and holds over 70 patents in the area of electromagnetics and wireless telecommunications. His current research interests include new tunable RF dielectric and optical media, RF filters, RF amplifiers, specialized antennas, complete RF transceivers, and a plethora of RF passive and active devices (attenuators, couplers, and phase shifters) up to 300 GHz.

Dr. Bulja is a Chartered Engineer, and a Full Member of the MTT-23 Wireless Communications Technical Committee. He was a recipient of many awards, such as the award for being Nokia's Top Inventor and Best Innovation Prize from the European Space Agency.



DMITRY KOZLOV (Member, IEEE) received the B.Sc. and M.Sc. degrees in radiophysics from Saint Petersburg Electrotechnical University LETI, St. Petersburg, Russia, in 2009 and 2011, respectively, and the Ph.D. degree in electronics and electrical engineering from Queen's University Belfast (QUB), Belfast, U.K., in 2016. He was a Marie Curie Early Stage Researcher with the Institute of Electronics, Communications and Information Technology, QUB, from 2013 to 2016. He is currently with Nokia Mobile Networks, Ulm, Germany. His primary research interests include microwave and antenna theory, including synthesis of antenna arrays, mechanisms of PIM generation in microwave passive and tunable devices, and wireless energy transfer systems.